

# Multibranch Autocorrelation Method for Doppler Estimation in Underwater Acoustic Channels

Jianghui Li<sup>✉</sup>, Student Member, IEEE, Yuriy V. Zakharov<sup>✉</sup>, Senior Member, IEEE,  
and Benjamin Henson<sup>✉</sup>, Student Member, IEEE

**Abstract**—In underwater acoustic (UWA) communications, Doppler estimation is one of the major stages in a receiver. Two Doppler estimation methods are often used: the cross-ambiguity function (CAF) method and the single-branch autocorrelation (SBA) method. The former results in accurate estimation but with a high complexity, whereas the latter is less complicated but also less accurate. In this paper, we propose and investigate a multi-branch autocorrelation (MBA) Doppler estimation method. The proposed method can be used in communication systems with periodically transmitted pilot signals or repetitive data transmission. For comparison of the Doppler estimation methods, we investigate an orthogonal frequency-division multiplexing (OFDM) communication system in multiple dynamic scenarios using the Waymark simulator, allowing virtual UWA signal transmission between moving transmitter and receiver. For the comparison, we also use the OFDM signals recorded in a sea trial. The comparison shows that the receiver with the proposed MBA Doppler estimation method outperforms the receiver with the SBA method and its detection performance is close to that of the receiver with the CAF method, but with a significantly lower complexity.

**Index Terms**—Ambiguity function, autocorrelation, Doppler estimation, orthogonal frequency-division multiplexing (OFDM), underwater acoustic (UWA) communications.

## I. INTRODUCTION

IN UNDERWATER acoustic (UWA) communications, due to the slow propagation speed of acoustic waves, the Doppler effect introduces significant distortions in propagated signals [2]–[5]. To achieve a high detection performance, accurate Doppler estimation and compensation techniques are required [2], [6]–[8]. The Doppler effect is caused by transmitter/receiver motion, by surface waves, by fluctuations of the sound speed, and other phenomena [9]–[11]. The Doppler effect on signals is often described as time compression/dilation with a compression factor constant over a measurement interval, i.e., a constant-speed movement [12]–[15]. For specific underwater tasks, such as underwater imaging, environment monitoring, and sea bottom searching, fast-moving platforms such as autonomous underwater vehicles (AUVs) can use

Manuscript received October 5, 2016; revised May 17, 2017 and October 2, 2017; accepted October 4, 2017. Date of publication November 1, 2017; date of current version October 11, 2018. This paper was presented in part at the Underwater Acoustics, Conference and Exhibition, Crete, Greece, June 21–26, 2015. (Corresponding author: Jianghui Li.)

**Associate Editor:** R. Diamant.

The authors are with the Department of Electronic Engineering, University of York, York YO10 5DD, U.K. (e-mail: jl1384@york.ac.uk; yury.zakharov@york.ac.uk; bth502@york.ac.uk).

Digital Object Identifier 10.1109/JOE.2017.2761478

complicated trajectories [16]–[21], where the constant-speed assumption is not valid. Such movements require frequent re-estimation of the Doppler effect to support a high detection performance of UWA communications [22]. The Doppler estimation then becomes a complicated task dominating the complexity of the receiver [23].

Many Doppler estimation methods are currently used in UWA communications. One such method involves transmitting Doppler-insensitive preamble and postamble around a data package and estimation of the time difference between their arrivals, transformed into the time-compression factor [2], [24], [25]. However, this method assumes that the time compression (the transmitter/receiver velocity) is constant over the data package, which is often not the case with a fast-moving and manoeuvring transmitter/receiver. With fast-varying movements, the Doppler estimation should also be performed within the data package, sometimes requiring updates with every received data symbol [22]. Such Doppler estimation techniques have been specifically developed for different single-carrier modulation schemes [7], [26]–[28]. However, these techniques cannot be directly applied to multicarrier transmission, such as the orthogonal frequency-division multiplexing (OFDM); besides, multicarrier schemes are more sensitive to Doppler distortions and require more accurate Doppler estimation [29].

One efficient method of Doppler estimation in multipath channels is based on computing the cross-ambiguity function (CAF) between received and transmitted signals [29]–[31]. The CAF is computed on a 2-D grid of channel delays and Doppler compression factors. The position of maximum of the CAF magnitude over the Doppler grid provides an estimate of the Doppler compression. However, due to a large number of Doppler estimation channels, the CAF method is computationally intensive, even if fast Fourier transforms (FFT) and a two-step (coarse and fine estimation) approach is used to reduce the number of Doppler channels and speed up the computations [8], [12], [23]. Significantly less complicated is the single-branch autocorrelation (SBA) method [12], [32]–[35]. This method is applied to periodic transmitted signals and it exploits the fact that with a moving transmitter/receiver, the signal period changes; the SBA method measures this change to estimate the time-compression factor. Apart from being of low complexity due to a single estimation branch, another benefit of this method is the efficient combining of multipath components. However, the method can fail in cases where the motion of transmitter/receiver involves accelerations.

In this paper, we propose a multibranch autocorrelation (MBA) [1] method that is capable of estimating the Doppler effect in UWA channels with fast moving and manoeuvring transmitter/receiver, having significantly lower complexity than the CAF method and outperforming the SBA method.

One of significant problems of testing signal processing algorithms for UWA communications is the modeling of the signal transmission, taking into consideration the specific time-varying multipath propagation due to the complicated motion of a receiver and transmitter. For such a virtual signal transmission, i.e., the transmission that mimics a real sea trial, the *VirTEX* underwater propagation channel model was developed [36] and used [37]; this model is based on the Bellhop ray/beam tracing [38] to compute the channel impulse response in different acoustic propagation environments. A similar approach was implemented in the Waymark model [10], [39], [40] developed to efficiently simulate the UWA signal transmission in long communication sessions. We use the Waymark model to test the Doppler estimation methods in communication sessions with complicated motion of the transmitter and receiver.

In this paper, the Doppler estimation methods are implemented in a communication system with guard-free OFDM and superimposed data and pilot signals [10], [30], [31], [41]. The comparison of the three methods (CAF, SBA, and MBA) in a number of simulation scenarios, as well as in a real sea trial, shows that the MBA method outperforms the SBA method; also its performance is comparable to that of the CAF method, but with lower complexity.

This paper is organized as follows. Section II describes the transmitted signal, channel model, and receiver. Section III presents the proposed MBA Doppler estimation method. Implementations of the CAF, SBA, and MBA methods are described in Section IV. Sections V and VI compare the Doppler estimators in multiple scenarios, using the Waymark model and data recorded in a sea trial, respectively. Section VII summarizes this paper.

## II. TRANSMITTED SIGNAL, CHANNEL MODEL, AND RECEIVER

In this section, the transmitted signal, the channel model, and the receiver structure are described. Transmitted signals that we consider here are guard-free OFDM signals with superimposed pilot signals [23]. However, the proposed Doppler estimation technique can operate with other types of transmitted signals, in which the same signal pattern is repeated in time.

The transmitted signal  $x(t)$  consists of a continuous sequence of guard-free OFDM symbols [23], [30]

$$x_l(t) = \Re \left\{ e^{j2\pi f_c t} \sum_{k=-N_s/2}^{N_s/2-1} [M_p(k) + jD_l(k)] e^{j\frac{2\pi}{T_s} kt} \right\} \quad (1)$$

where  $l = 1, 2, \dots, L$ ,  $L$  is the number of OFDM symbols in the transmitted data package,  $N_s = 1024$  is the number of subcarriers,  $f_c = \omega_c/(2\pi) = 3072$  Hz is the carrier frequency,  $F = 1024$  Hz is the frequency bandwidth,  $T_s = 1$  s is the symbol duration, and  $j = \sqrt{-1}$ . Sequence  $M_p(k) \in [-1, +1]$  is a binary pseudorandom sequence of length  $N_s$ , serving as the

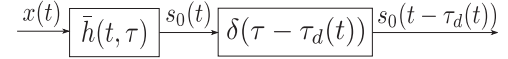


Fig. 1. Channel model.

superimposed pilot signal, the same for all OFDM symbols. Therefore, the pilot signal is periodic in time with period  $T_s$ . Sequence  $D_l(k)$  represents the information data in the  $l$ th OFDM symbol; it is obtained by interleaving and encoding original data across subcarriers using rate 1/2 convolutional codes [42].

The UWA channel is often modeled as a time-variant linear system with an impulse response  $h(t, \tau)$  that describes multipath and Doppler spreads in the channel. The received signal is then given by

$$r(t) = \int_{-\infty}^{\infty} h(t, \tau) x(t - \tau) d\tau + \nu(t) \quad (2)$$

where  $\nu(t)$  is the additive noise. In UWA communications, for a general time-varying multipath channel, different propagation paths, corresponding to different delays  $\tau$ , might have different Doppler compression factors. The channel can be represented using two time-varying components described by a dominant time-varying channel delay  $\tau_d(t)$  and a slower time-varying channel impulse response  $\bar{h}(t, \tau)$ , as shown in Fig. 1 [23]. Component  $\delta(\tau - \tau_d(t))$ , where  $\delta(\tau)$  is the Dirac delta function, can be thought of as caused by the varying distance between the transmitter and the receiver. The component  $\bar{h}(t, \tau)$  incorporates differential variations in the lengths of acoustic rays due to the movement. Thus, the time-varying channel impulse response  $h(t, \tau)$  can be represented as a convolution of  $\delta(\tau - \tau_d(t))$  and  $\bar{h}(t, \tau)$ . Therefore, the received signal can be represented as  $r(t) = s(t) + \nu(t)$ , where  $s(t) = s_0(t - \tau_d(t))$  and  $s_0(t) = \int_{-\infty}^{\infty} \bar{h}(t, \tau) x(t - \tau) d\tau$ .

The channel model in Fig. 1 is useful for designing receivers in scenarios with a fast moving transmitter and/or receiver. The channel component described by the dominant time-varying delay  $\tau_d(t)$  is associated with fastest channel variations, since a small variation in the delay results in a significant variation in the phase of the received signal. However, this component can be described by a few parameters [4], [5]. Therefore, it can be accurately estimated using a Doppler estimator, such as the estimator based on calculation of the ambiguity function [29]–[31] or the autocorrelation [12], [32]–[35], and further equalized using resampling. The other component of the channel representation, described by the impulse response  $\bar{h}(t, \tau)$ , still contains most of the parameters to be estimated, such as the multipath delays and complex amplitudes. However, these parameters are slower varying in time compared to that of the channel response  $h(t, \tau)$ . Therefore, an equalizer for the channel component  $\bar{h}(t, \tau)$  is easier to build than an equalizer for the channel response  $h(t, \tau)$ . Many practical receivers are built using this approach, where parameters of the dominant time-varying delay  $\tau_d(t)$  are estimated using a Doppler estimator and equalized by resampling the received signal. After that the channel component  $\bar{h}(t, \tau)$  is equalized, e.g., using a linear

equalizer. For more discussion on this channel representation, see [10] and [23].

Below, when deriving the proposed MBA Doppler estimator, we will assume that, on the estimation time interval, the impulse response  $\bar{h}(t, \tau)$  is time invariant, i.e.,  $\bar{h}(t, \tau) = \bar{h}(\tau)$ , and that the time-varying delay  $\tau_d(t)$  is described by a quadratic polynomial; see (9). However, when testing this and other Doppler estimators, we will be using more realistic scenarios, with different propagation paths having different Doppler spreads. Note that the scenarios will be defined by the acoustic environment and trajectory of the transmitter/receiver. In the test scenarios, the impulse response  $h(t, \tau)$  is incorporated into the data obtained either in a real sea experiment or via virtual signal transmission using the Waymark simulator [10], [39]. Therefore, the channel parameters, including the Doppler parameters associated with the dominant time-varying channel delay  $\tau_d(t)$ , are not explicitly available for comparison with their estimates. Besides, there are possible multiple variants of splitting  $h(t, \tau)$  into the two components  $\bar{h}(t, \tau)$  and  $\tau_d(t)$ . Therefore, we will be assessing the performance of Doppler estimators by comparing the detection performance of a receiver using these estimators.

Fig. 2 shows the block diagram of the receiver. The front-end processing implements the frequency shifting of the received signal  $r(t) = s(t) + \nu(t)$  by  $\omega_c$ , the lowpass filtering, and analog-to-digital conversion of the baseband signal

$$\tilde{r}(t) = \tilde{s}(t) + \tilde{\nu}(t)$$

where  $\tilde{\nu}(t)$  is a baseband noise signal, into signal samples  $\tilde{r}(n)$  taken with a sampling interval  $\Delta\tau = T_s/(N_s N_\tau)$ , where  $N_\tau$  is the time oversampling factor, which is set to  $N_\tau = 2$  for our experiments.

The Doppler estimation consists of two steps: coarse and fine estimation. The coarse estimation is implemented using one of three methods: CAF, SBA, or MBA. The coarse Doppler estimation is performed on a coarse grid of Doppler scaling factors. However, this coarse resolution is not good enough for equalization and demodulation. Therefore, the coarse estimate is refined by using parabolic interpolation as detailed in [23]. The discrete-time estimates of the Doppler scale factor obtained with the time interval  $T_{\text{est}}$  (in our experiments,  $T_{\text{est}} = T_s/4$ ) are linearly interpolated, and used to compensate for the dominant time-varying Doppler effect by resampling and frequency correcting the signal  $\tilde{r}(n)$  (see [23] for details).

The resampled and frequency corrected signal  $\tilde{r}(n)$  is divided into two diversity signals, corresponding to odd and even samples of  $\tilde{r}(n)$ , respectively. The two signals are independently time-domain equalized. Assuming perfect compensation of the dominant Doppler compression described by the time-varying delay  $\tau_d(t)$ , the equalization deals with the distortions of the signal caused by the slow variant impulse response  $\bar{h}(t, \tau)$  (see Fig. 1). The equalized signals from the two diversity branches are combined and demodulated to produce tentative data estimates, further refined in  $Q$  turbo iterations; in our experiments,  $Q = 1$ . The final data estimate  $D^{(Q)}$  are applied to the Viterbi decoder [42] to recover transmitted data.

More details on the operation of the receiver shown in Fig. 2 can be found in [23]. In [23], the CAF Doppler estimator is

implemented. It has high complexity, which is the largest contribution to the total receiver complexity. In this paper, we propose a multibranch Doppler estimator that has significantly lower complexity and provides almost the same detection performance as the CAF estimator.

### III. MULTIBRANCH AUTOCORRELATION DOPPLER ESTIMATOR

Consider the channel model in Fig. 1. Let the transmitted signal  $x(t)$  be represented using an equivalent baseband signal  $\tilde{x}(t)$

$$\begin{aligned} x(t) &= \Re\{\tilde{x}(t)e^{j\omega_c t}\} \\ &= \frac{1}{2}\tilde{x}(t)e^{j\omega_c t} + \frac{1}{2}\tilde{x}^*(t)e^{-j\omega_c t} \end{aligned} \quad (3)$$

where  $\Re\{\cdot\}$  denotes the real part and  $(\cdot)^*$  is the complex conjugate of a complex-valued number. Similarly, we have

$$\begin{aligned} s_0(t) &= \Re\{\tilde{s}_0(t)e^{j\omega_c t}\} \\ &= \frac{1}{2}\tilde{s}_0(t)e^{j\omega_c t} + \frac{1}{2}\tilde{s}_0^*(t)e^{-j\omega_c t} \end{aligned} \quad (4)$$

where  $\tilde{s}_0(t)$  is an equivalent baseband signal for  $s_0(t)$ .

Let the signal  $\tilde{x}(t)$  be periodic with a period  $T_s$  so that

$$\tilde{x}(t + T_s) = \tilde{x}(t).$$

Assume that the first component in the channel model, shown in Fig. 1, is time invariant, i.e.,  $\bar{h}(t, \tau) = \bar{h}(\tau)$ . Then, the baseband signal  $\tilde{s}_0(t)$  is also periodic with the same period  $T_s$ , i.e.,

$$\tilde{s}_0(t + T_s) = \tilde{s}_0(t).$$

The second channel component in Fig. 1 is modeled as a time-varying delay  $\tau_d(t)$ , so the output of the channel without noise is given by

$$\begin{aligned} s(t) &= s_0(t - \tau_d(t)) \\ &= \frac{1}{2}\tilde{s}_0(t - \tau_d(t))e^{j\omega_c(t - \tau_d(t))} \\ &\quad + \frac{1}{2}\tilde{s}_0^*(t - \tau_d(t))e^{-j\omega_c(t - \tau_d(t))}. \end{aligned} \quad (5)$$

In a receiver, typical front-end processing includes a frequency shifting of the received signal  $s(t)$  by  $\omega_c$  via multiplying the signal by  $e^{-j\omega_c t}$  and further lowpass filtering. Therefore, the second component in (5) is filtered out, and the front-end processing produces a baseband signal

$$\tilde{s}(t) = \tilde{s}_0(t - \tau_d(t))e^{-j\omega_c \tau_d(t)}. \quad (6)$$

#### A. Single-Branch Autocorrelation Estimator

The delay  $\tau_d(t)$  can often be represented as a linear function of time, described by two parameters, an initial delay  $a_0$  and a time-compression factor  $a_1$  [4], [5] as

$$\tau_d(t) = a_0 + a_1 t, \quad t \in [-\Theta/2, \Theta/2]$$

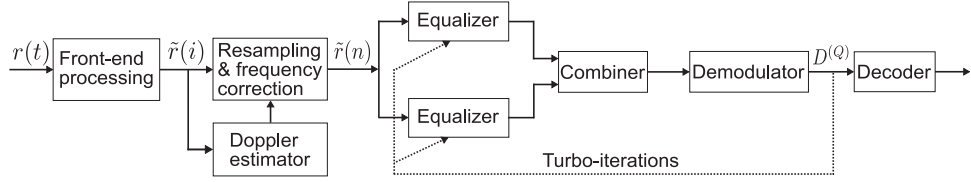


Fig. 2. Block diagram of the receiver for guard-free OFDM signals.

where  $\Theta$  is a measurement interval. For estimation of the parameter  $a_1$ , the autocorrelation function

$$\rho(\tau) = \int_{-\Theta/2}^{\Theta/2} \tilde{s}^*(t)\tilde{s}(t+\tau)dt \quad (7)$$

of the baseband signal  $\tilde{s}(t)$  can then be used [43]. More specifically,  $a_1$  can be estimated by searching for the maximum of  $|\rho(\tau)|$  over delays near the signal period  $T_s$

$$\tau_{\max} = \arg \max_{T_s - \tau_M \leq \tau \leq T_s + \tau_M} |\rho(\tau)| \quad (8)$$

where  $[T_s - \tau_M, T_s + \tau_M]$  is a search interval defined by the maximum possible delay  $\tau_M$  due to the time compression, i.e., due to the maximum relative velocity between the transmitter and the receiver. The ratio  $\hat{a}_1 = 1 - T_s/\tau_{\max}$  can be considered as an estimate of  $a_1$  (see below). We call such an estimator of  $a_1$  the SBA estimator.

### B. Multibranch Autocorrelation Estimator

However, the SBA estimator is limited in accuracy when the Doppler compression factor varies over the measurement interval, i.e., when the delay line in Fig. 1 is described by a polynomial of a higher degree, e.g., if  $\tau_d(t)$  is a quadratic polynomial

$$\tau_d(t) = a_0 + a_1 t + a_2 t^2, \quad t \in [-\Theta/2, \Theta/2] \quad (9)$$

where  $a_2$  is a parameter describing the acceleration. Let  $a$  be an acceleration between the transmitter and receiver. Due to this acceleration, the distance  $d(t)$  between the transmitter and the receiver varies in time as  $d(t) = at^2/2$ . Since  $\tau_d(t) = d(t)/c$ , we have  $a_2 = a/(2c)$ , where  $c$  is the sound speed.

In fast-varying channels, for estimation of Doppler parameters, we propose to use the following statistic:

$$\rho(\tau, \Omega, \mu) = \int_{-\Theta/2}^{\Theta/2} \tilde{s}^*(t)\tilde{s}(\mu t + \tau)e^{j\Omega t} dt. \quad (10)$$

Specifically, the position of the peak of  $|\rho(\tau, \Omega, \mu)|$  over delay  $\tau$  near the signal period  $T_s$  and over frequency  $\Omega$  and compression factor  $\mu$

$$\{\tau_{\max}, \Omega_{\max}, \mu_{\max}\} = \arg \max_{\tau, \Omega, \mu} |\rho(\tau, \Omega, \mu)| \quad (11)$$

will define the Doppler estimate as explained in Appendix A. More specifically, it is shown that the parameter  $a_1$  can be estimated as

$$\hat{a}_1 = 1 - \frac{T_s}{\tau_{\max}} - \alpha \frac{\Omega_{\max}}{2\omega_c} \quad (12)$$

where  $\alpha = [\Theta/(k\tau_{\max})]^2 \simeq 1$  and  $k = 1 - a_1$ . The parameter  $a_2$  can be estimated as

$$\hat{a}_2 = \frac{\Omega_{\max} + a_1(1 - \mu_{\max})\omega_c}{2\mu_{\max}\tau_{\max}\omega_c} \quad (13)$$

where instead of  $a_1$ , its estimate  $\hat{a}_1$  can be substituted. Since in many scenarios,  $\mu_{\max} \approx 1$ , the estimate in (13) can be simplified and made independent of  $a_1$

$$\hat{a}_2 = \frac{\Omega_{\max}}{2\tau_{\max}\omega_c}. \quad (14)$$

The values  $\mu_{\max}$  and  $\Omega_{\max}$  are interdependent as

$$\mu_{\max} = 1 + \frac{\Omega_{\max}}{\omega_c}. \quad (15)$$

This simplifies the Doppler estimation. According to (11), the statistic  $|\rho(\tau, \Omega, \mu)|$  needs to be computed at a 3-D grid. However, due to the interdependence, a 2-D grid over  $(\tau, \Omega)$  is sufficient.

If  $\Theta\Omega_{\max}/\omega_c < 1$ , we can set  $\mu = 1$  in (10), i.e., the resampling is not required, thus further simplifying the signal processing. With high accelerations  $a$  and high values of the measurement interval  $\Theta$  and/or frequency bandwidth  $F$ , one of the components in (10) will need to be prescaled with a compression factor  $\mu$  related to the frequency  $\Omega$  as  $\mu = 1 + \Omega/\omega_c$ . In our scenarios, this requirement is satisfied for the whole range of  $\Omega$ , and therefore, we set  $\mu = 1$ , thus avoiding the resampling.

The estimates of parameters  $a_1$  and  $a_2$ , obtained in the MBA Doppler estimator, are used for approximation of the delay  $\tau_d(t)$  and resampling of the received signal (see Fig. 2).

Note that in the SBA method, the term  $\alpha\Omega_{\max}/(2\omega_c)$  as in (12) is ignored, which makes the SBA method less accurate when there is a nonzero acceleration  $a$ . However, the main disadvantage of the SBA method compared to the MBA method is that with nonzero acceleration, the amplitude of the autocorrelation peak about the signal period  $T_s$  is reduced. For example, for pseudonoise signals, such as the  $m$ -sequence [42], with a  $\delta$ -like ambiguity function, the amplitude at  $\Omega = 0$  will be close to zero if  $\Omega_{\max}\Theta > 2\pi$ ; for example, for our scenarios, it corresponds to accelerations  $a > 0.5 \text{ m/s}^2$ .

## IV. IMPLEMENTATION OF DOPPLER ESTIMATORS

### A. Implementation of Cross-Ambiguity Function Method

In the CAF method,  $2N_d + 1$  Doppler sections of the ambiguity function are computed with a period  $T_{\text{est}}$  by cross correlating the scale-distorted received signal and one period of the pilot signal (see [2] and [23] for more details). The ambiguity

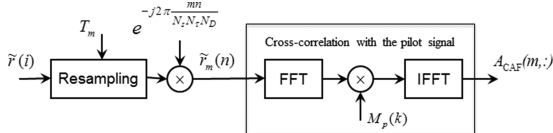


Fig. 3. Computation of one Doppler section of the CAF.

function is computed on the delay-Doppler scale grid. The delay step on the grid is  $\Delta\tau$ . The Doppler scale step is chosen so that the corresponding frequency shift  $\Delta f$  is a predefined fraction of the subcarrier spacing  $F/N_s$ :  $\Delta f = F/(N_s N_D)$ , with the frequency oversampling factor  $N_D$  set to  $N_D = 2$ . In [23], it is shown that such a coarse resolution is enough for operation of the receiver, whereas higher  $N_D$  would proportionally increase the complexity of the Doppler estimator.

To cover the whole Doppler spread, the CAF  $A_{\text{CAF}}(m, n)$ ,  $m = -N_d, \dots, N_d$ ,  $n = 0, \dots, N_s N_\tau - 1$ , has  $2N_d + 1$  Doppler sections. The  $\hat{m}$ th Doppler section with the maximum magnitude indicates the coarse Doppler estimate

$$[\hat{m}, \hat{n}] = \arg \max_{m, n} |A_{\text{CAF}}(m, n)|.$$

One Doppler section  $A_{\text{CAF}}(m, :)$  is computed, as shown in Fig. 3. The input signal  $\tilde{r}(i)$  with the original sampling rate  $f_s$  is resampled and frequency shifted according to the  $m$ th scale factor  $1 + d(m)$ , where  $d(m) = m\Delta f/f_c = mF/(N_s N_D f_c)$  and  $m = -N_d, \dots, N_d$ . The resampling interval  $T_m$  for the  $m$ th Doppler section is given by  $T_m = 1/[FN_\tau(1 + d(m))]$ . The resampling is based on the linear interpolation and compensates for the time scale with the factor  $1 + d(m)$ .

Denoting  $\hat{r}(t)$  as a continuous-time signal that would be obtained via the linear interpolation of  $\tilde{r}(i)$ , after the resampling and frequency correction, we have  $\tilde{r}_m(n) = \hat{r}(nT_m) \exp(-j2\pi mn/N_s N_\tau N_D)$ . Such a Doppler-like distorted received signal is correlated with one period of the pilot signal  $p(i)$  as

$$A_{\text{CAF}}(m, n) = \sum_{i=0}^{N_\tau N_s - 1} \tilde{r}_m(i) p^*(i \oplus n) \quad (16)$$

where  $\oplus$  denotes the cyclic shift over the period  $N_s N_\tau$ ,  $(\cdot)^*$  denotes complex conjugate, and

$$p(i) = \sum_{k=-N_s/2}^{N_s/2-1} M_p(k) e^{-j\frac{2\pi}{N_s N_\tau} ki}. \quad (17)$$

This computation can be done using FFT and inverse FFT (IFFT), as shown in Fig. 3. The use of FFT and IFFT for computing the cross correlation is possible because OFDM symbols have no guard interval, the pilot signal is periodic, and the orthogonality interval is equal to the OFDM symbol duration. The position of the peak of the CAF magnitude indicates the coarse Doppler estimate:  $\hat{a}_1 = -d(\hat{m})/[1 + d(\hat{m})]$ . The FFT in Fig. 3 is of size  $N_s N_\tau$ ; such a time oversampling allows avoiding the interference at boundary subcarriers (close to the frequencies  $f_c - F/2$  and  $f_c + F/2$ ). Although the frequency-domain multiplication by the pilot sequence  $M_p(k)$ ,  $k = 0, \dots, N_s - 1$ , is

only over  $N_s$  subcarriers, the IFFT in Fig. 3 is also of size  $N_s N_\tau$  with zero padding of the rest  $N_s(N_\tau - 1)$  FFT bins; this provides more accurate position estimation for the peak of the ambiguity function.

### B. Implementation of the Single-Branch Autocorrelation Method

The SBA method is implemented by computing the autocorrelation of the received signal as

$$A_{\text{SBA}}(\tau) = \sum_{i=0}^{N_\tau N_s - 1} \tilde{r}^*(i) \tilde{r}\left(i + \frac{\tau}{\Delta\tau}\right) \quad (18)$$

where  $\tau/\Delta\tau \in \{N_\tau N_s - \tau_M/\Delta\tau, N_\tau N_s + \tau_M/\Delta\tau\}$ , and finding the maximum

$$\tau_{\max} = \arg \max_{\tau} |A_{\text{SBA}}(\tau)|.$$

The parameter  $a_1$  is then estimated as in (12) with  $\Omega_{\max} = 0$ .

### C. Implementation of Multibranch Autocorrelation Method

The MBA method is implemented by computing  $2N_d + 1$  autocorrelation functions with a set of frequency shifts  $\Omega_m$ ,  $m = -N_d, \dots, N_d$  as follows:

$$A_{\text{MBA}}(\tau, \Omega_m) = \sum_{i=0}^{N_\tau N_s - 1} \tilde{r}^*(i) \tilde{r}\left(i + \frac{\tau}{\Delta\tau}\right) e^{j\Omega_m \Delta\tau i} \quad (19)$$

where  $\tau/\Delta\tau \in \{N_\tau N_s - \tau_M/\Delta\tau, N_\tau N_s + \tau_M/\Delta\tau\}$  and  $\Omega_m = 2\pi\Delta f m$ . The parameter  $a_1$  is then estimated as in (12) with  $\alpha = 1$  and  $a_2$  is estimated as in (14), where

$$\{\tau_{\max}, \Omega_{\max}\} = \arg \max_{\tau, \Omega_m} |A_{\text{MBA}}(\tau, \Omega_m)|.$$

Note that the complexity of each of the three methods is directly proportional to the number of Doppler estimation sections ( $2N_d + 1$ ). It is shown in Appendix B that the complexity of computing a single Doppler section is approximately the same in all the methods. Therefore, to compare the complexity, we need to know the number of Doppler sections. The SBA method is the simplest one since it requires a single Doppler section,  $N_d = 1$ . For the CAF method,  $N_d$  is approximately given by

$$N_d = \text{round} \left[ \frac{V_{\max} f_c}{c \Delta f} \right] \quad (20)$$

where  $\text{round}[\cdot]$  denotes the closest integer number,  $\Delta f = 0.5$  Hz is the Doppler frequency step,  $f_c = 3072$  Hz is the carrier frequency,  $c = 1500$  m/s is the underwater sound speed, and  $V_{\max}$  is the maximum speed of the transmitter/receiver. The MBA method is an extension of the SBA method as (19) is an extension of (18). Since with (19), the 1-D search is replaced with a 2-D search, the complexity of the MBA method is higher than that of the SBA method. For the MBA method,  $N_d$  is given by

$$N_d = \text{round} \left[ \frac{U_{\max} T_s f_c}{c \Delta f} \right] \quad (21)$$

where  $U_{\max}$  is the maximum acceleration of the transmitter/receiver. In typical scenarios,  $U_{\max} T_s < V_{\max}$ , and therefore,

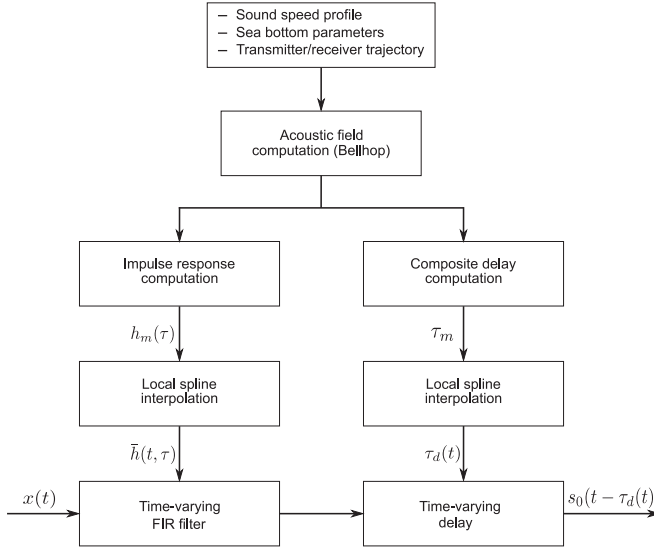


Fig. 4. Block diagram of the Waymark UWA simulator.

the number of Doppler sections  $N_d$  in the MBA method is typically smaller than  $N_d$  in the CAF method, as can be seen from comparison of (20) and (21), thus reducing the complexity of the MBA method.

## V. NUMERICAL RESULTS

In this section, we investigate the detection performance of three versions of the receiver of guard-free OFDM signals, shown in Fig. 2. These versions differ in the Doppler estimator, which are the CAF, SBA, or MBA estimator. The investigation is performed using the Waymark simulator [10], [39], [40] to model the time-varying multipath distortions of signals, caused by moving transmitter and/or receiver in specific acoustic environments. The required signal-to-noise ratio (SNR), from 7 to 17 dB, is then achieved by adding independent Gaussian noise to the distorted signal. The SNR is defined as the ratio of the energy of the distorted signal over the whole length of the communication session to the noise energy over the same time interval, in the frequency bandwidth of the transmitted signal (from 2560 to 3584 Hz).

The Waymark channel simulator [10], [39], [40] shown in Fig. 4 implements the channel model in Fig. 1 using the acoustic field computation for an environment defined by a sound-speed profile (SSP) and acoustic bottom parameters. This is done using the Bellhop ray/beam tracing [38]. Using the ray parameters, the Waymark simulator computes the dominant delays  $\{\tau_m\}$  and channel impulse responses  $\{h_m(\tau)\}$  for a set of points (waymarks) along the transmitter/receiver trajectory. These are spline interpolated in time to obtain the continuous time-varying delay  $\tau_d(t)$  and impulse response  $\bar{h}(t, \tau)$ ; in the simulator, the continuous time  $t$  is treated as the discrete time at a sampling rate high enough to accurately represent the communication signal. The (fractional) delay  $\tau_d(t)$  is then implemented by interpolation of the signals, whereas the convolution with the impulse response  $\bar{h}(t, \tau)$  is implemented using a time-varying

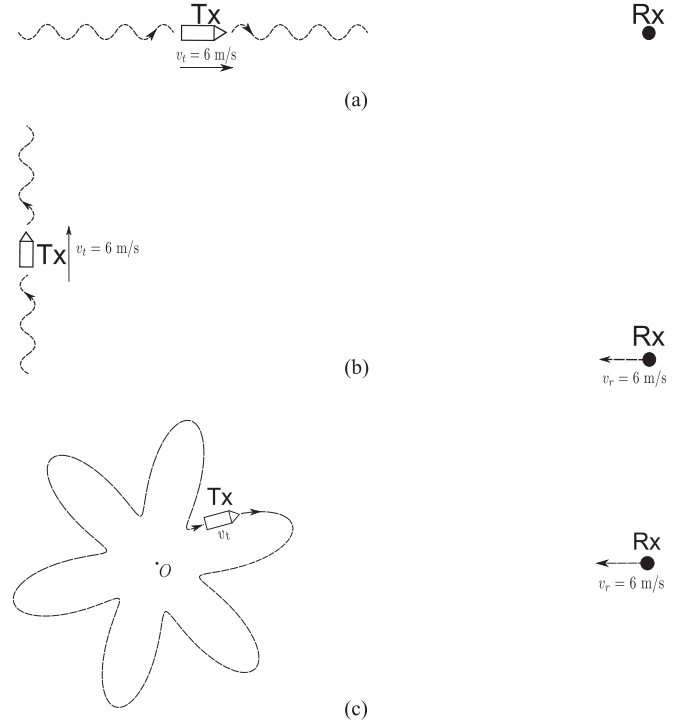


Fig. 5. Simulation scenarios (top view; Tx is the transmitter, and Rx is the receiver). (a) Transmitter moves toward receiver (Scenario 1). (b) Transmitter moves past receiver (Scenario 2). (c) Flower circle movement of the transmitter; O is the center of the flower (Scenario 3).

finite impulse response (FIR) filter. In this paper, the Waymark simulator is used for numerical investigation of the Doppler estimation methods in a number of scenarios. Note that sea trials with such scenarios would otherwise be difficult to conduct. However, data from a sea trial are also used for investigation of the Doppler estimators, see Section VI.

In the Waymark simulation, the following three scenarios are considered.

- 1) *Scenario 1:* The transmitter moves with a sinusoid-like trajectory toward the receiver at a speed of 6 m/s, while the receiver is stationary, as shown in Fig. 5(a).
- 2) *Scenario 2:* The transmitter moves with a sinusoid-like trajectory past the receiver at a speed of 6 m/s, while the receiver moves toward the transmitter at a speed of 6 m/s, as shown in Fig. 5(b).
- 3) *Scenario 3:* The transmitter performs a slow *flower circle* movement, while the receiver moves towards the transmitter at a speed of 6 m/s, as shown in Fig. 5(c).

The depth of both the transmitter and the receiver is 60 m. The data transmission last for 200 s, i.e.,  $L = 200$  OFDM symbols are transmitted in a communication session.

### A. Scenario 1

In this scenario, two shallow water environments are considered, with summer and winter SSPs [44], [45], shown in Fig. 6(a) and (b), respectively. The transmitter moves toward the receiver with a sinusoid-like trajectory, as shown in Fig. 5(a).

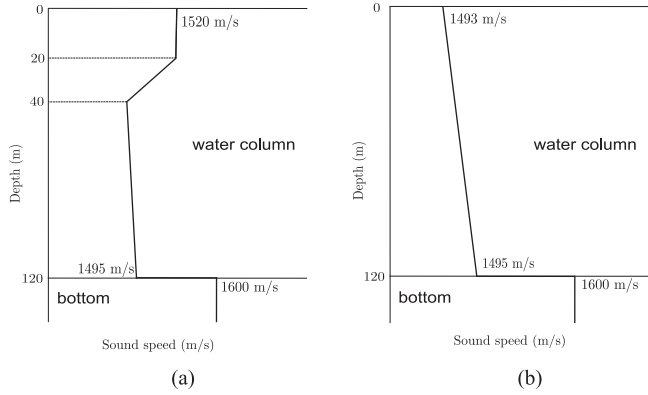


Fig. 6. Shallow water SSPs [44], [45] used in the simulation. (a) Summer SSP. (b) Winter SSP.

Such a movement can be caused when a transducer is towed by a surface vessel. Indeed, the sinusoid-like trajectory is only an approximation of a real movement affected by the surface waves [10]. The distance  $D(t)$  between the transmitter and the receiver varies in time as

$$D(t) = D_0 - v_t t + K \sin\left(\frac{2\pi t}{T}\right) \quad (22)$$

where  $D_0$  is an initial distance at  $t = 0$ ,  $K = 2$  m is the sinusoid amplitude,  $T = 10$  s is a typical period of surface waves, and  $v_t = 6$  m/s is the speed of the vessel. Thus, the maximum speed between the transmitter and receiver is  $V_{\max} = 7.3$  m/s and the maximum acceleration is  $U_{\max} = 0.79$  m/s<sup>2</sup>.

Based on the maximum velocity and acceleration, from (20) and (21) we obtain the number of Doppler sections in the CAF and MBA estimators as 61 and 7, respectively. As the complexity of the estimators is proportional to the number of Doppler sections, it can be seen that the MBA estimator requires almost nine times less computations. Indeed, the SBA method requires a single Doppler section and it has the lowest complexity of the three methods. However, as will be seen from our investigation, the SBA method is incapable of providing reliable detection.

1) *Experiment With the Summer Sound-Speed Profile:* This experiment starts at the distance  $D_0 = 10$  km. Fig. 7(a) shows fluctuations of the channel impulse response. Fig. 8(a) shows the bit-error-rate (BER) performance of the receiver with the three Doppler estimation methods. It can be seen that the SBA method is unable to provide a reliable detection, whereas the MBA estimator provides a BER performance comparable to that of the CAF method.

2) *Experiment With the Winter Sound-Speed Profile:* In this case, the SSP is as shown in Fig. 6(b), and the initial distance is set to  $D_0 = 20$  km. Fig. 7(b) shows fluctuations of the channel impulse response in this case. It is seen that the multipath structure of this channel is more complicated than in the channel with the summer SSP. However, as seen in Fig. 8(b), the proposed MBA method still provides a performance comparable to that of the CAF method. It is also seen that the SBA method cannot provide reliable detection.

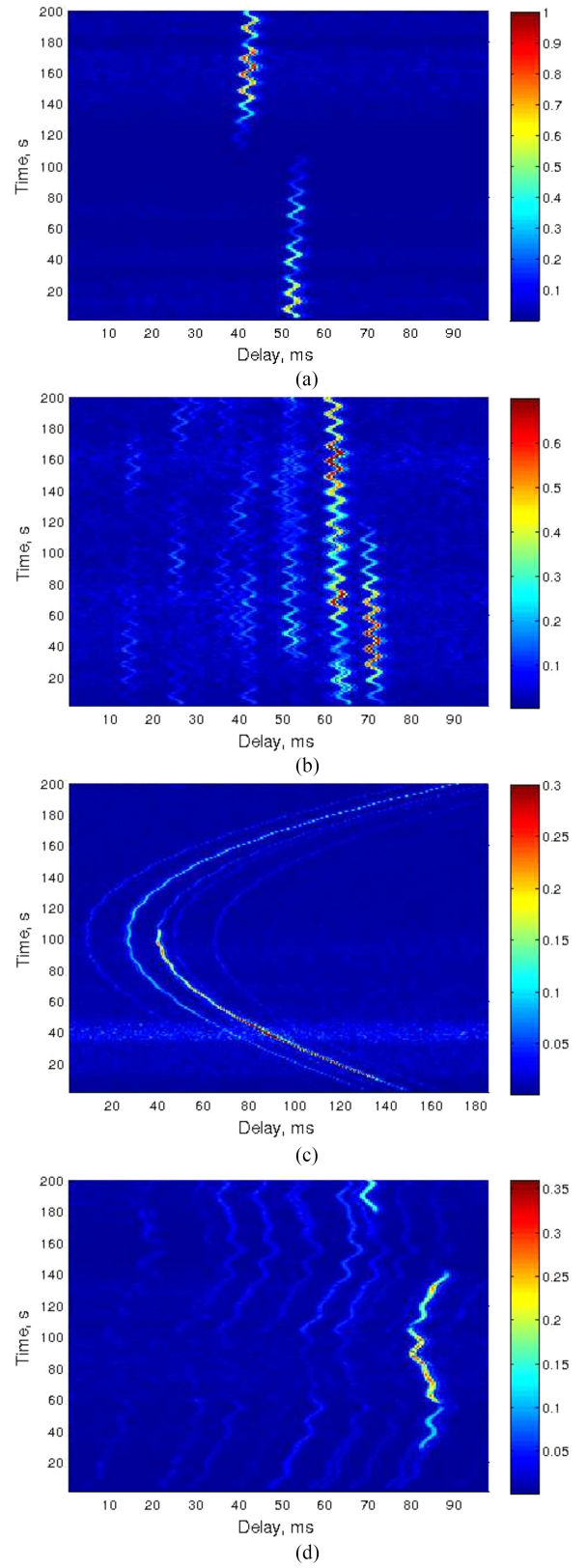


Fig. 7. Fluctuations of the channel impulse response in the four simulation scenarios (distance). (a) Summer SSP, transmitter moves toward receiver (10 km, Scenario 1). (b) Winter SSP, transmitter moves toward receiver (20 km, Scenario 1). (c) Summer SSP, transmitter moves past receiver (2 km, Scenario 2). (d) Summer SSP, flower circle movement (5 km, Scenario 3).

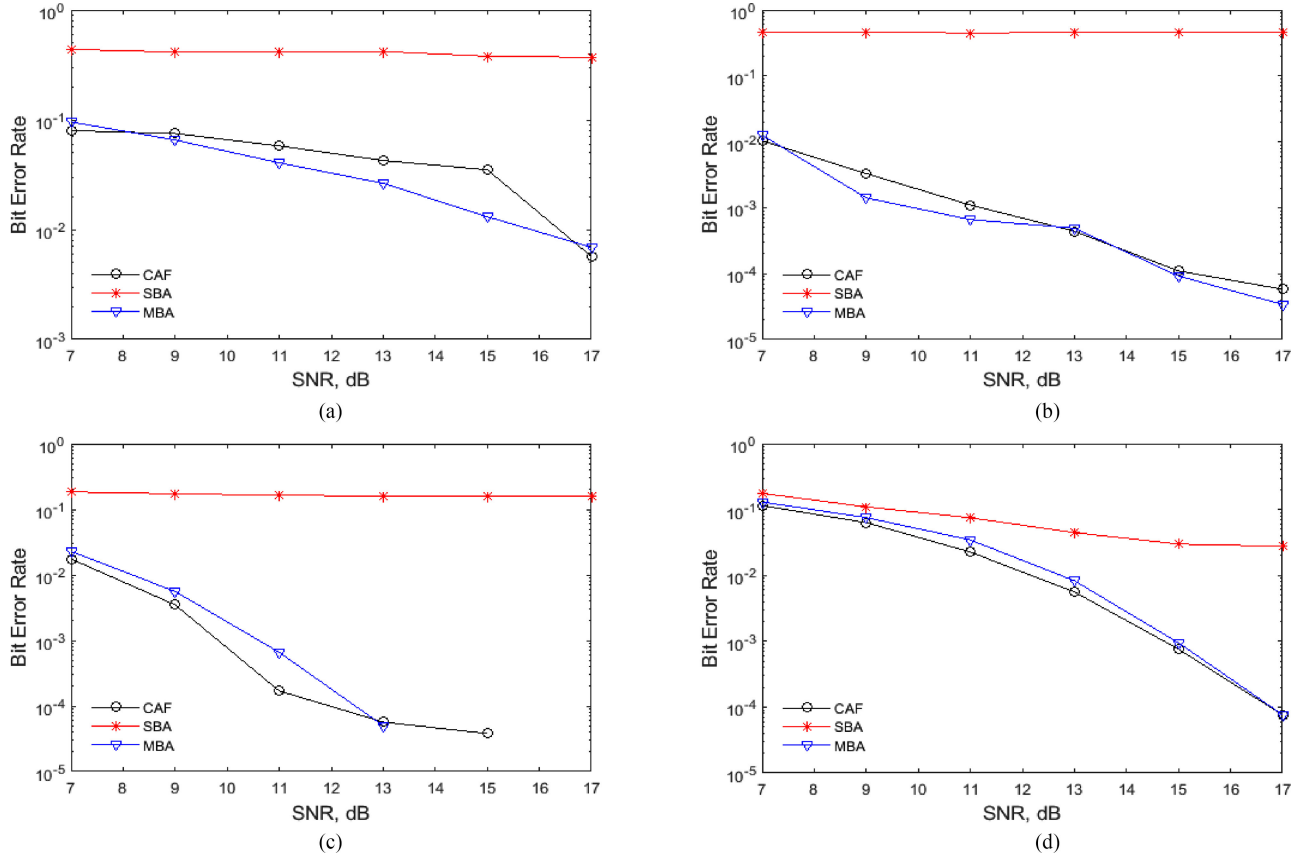


Fig. 8. BER performance of the receiver with the three Doppler estimation methods in the four simulation scenarios (environment, scenario, distance, data rate). (a) Summer SSP, transmitter moves toward receiver, 10 km, 1/2 b/s/Hz. (b) Winter SSP, transmitter moves toward receiver, 20 km, 1/2 b/s/Hz. (c) Summer SSP, transmitter moves past receiver, 2 km, 1/3 b/s/Hz. (d) Summer SSP, flower circle movement, 5 km, 1/3 b/s/Hz.

### B. Scenario 2

In this scenario, the summer SSP is used for simulation, and the distance  $D(t)$  between the transmitter and receiver is described as

$$D(t) = \sqrt{(D_0 - v_r t)^2 + (v_t t + K \sin(2\pi t/T))^2} \quad (23)$$

where  $D_0 = 2$  km is the initial distance at  $t = 0$ ,  $K = 2$  m,  $T = 10$  s, and  $v_t = v_r = 6$  m/s. Fig. 7(c) shows fluctuations of the channel impulse response in this scenario. Fig. 8(c) shows the BER performance of the receiver with the three Doppler estimation methods. It can be seen that, at SNRs higher than 15 dB, the CAF method provides error-free transmission, while the MBA method allows the error-free transmission at SNRs higher than 13 dB. It can also be seen that the SBA method shows poor performance, whereas the MBA estimator again shows a performance similar to that of the CAF method.

In this scenario, the maximum transmitter/receiver velocity is  $V_{\max} = 6$  m/s and the maximum acceleration is  $U_{\max} = 0.7$  m/s<sup>2</sup>. From (20) and (21), we obtain that the CAF method requires 51 Doppler sections and the MBA method requires seven Doppler sections, i.e., the MBA method requires about seven times less computations than the CAF method.

### C. Scenario 3

AUVs can use complicated trajectories for underwater imaging, monitoring, and sea bottom searching [16]–[21]. A complicated trajectory is considered in this scenario, as shown in Fig. 5(c); the trajectory of the transmitter looks like a petaled flower. The receiver moves at a speed of  $v_r = 6$  m/s. The distance  $D(t)$  between the transmitter and receiver is described as

$$\begin{aligned} D(t) = & \sqrt{(D_0 - v_r t)^2 + [K \sin(12\pi t/T) + 2]^2} \\ & - 2(D_0 - v_r t)[K \sin(12\pi t/T) + 2] \cos(2\pi t/T) \end{aligned} \quad (24)$$

where  $D_0 = 5$  km is the initial distance at  $t = 0$  between the central point [point  $O$  in Fig. 5(c)] of the flower and receiver,  $K = 2$  m, and  $T = 100$  s is the period of passing one flower circle; the external radius of the flower is 3 m.

Fig. 7(d) shows fluctuations of the channel impulse response in this scenario and Fig. 8(d) shows the BER performance of the receiver. It can be seen that the SBA method is outperformed by the other two methods, which show similar performance.

In this scenario, the transmitter moves with a relatively low time-varying velocity,  $v_t \leq 0.38$  m/s. The maximum transmitter/receiver velocity is  $V_{\max} = 6.8$  m/s, and the maximum acceleration is  $U_{\max} = 0.29$  m/s<sup>2</sup>. From (20) and (21), we obtain

that the CAF method requires 59 Doppler sections and the MBA method requires only 3 Doppler sections; thus, the MBA method has almost 20 times less complexity than the CAF method.

From this numerical investigation, we can conclude that the proposed MBA method significantly outperforms the SBA method. In fact, the BER performance achieved with the SBA method does not improve with increased SNR. This is explained by the fact that under a high acceleration, the received signal at delays close to  $T_s$  is decorrelated. Fig. 12(b) shows that, without the frequency correction (as in Doppler section 4), the autocorrelation peak is close to zero. However, with the frequency correction (as in Doppler section 2), the high autocorrelation is recovered. Therefore, in channels with high acceleration, the SBA method is not capable of providing a reliable detection, while the MBA method shows a high performance. It can also be seen that the MBA method provides a performance similar to that of the CAF method. However, the complexity of the MBA method is significantly lower than the CAF complexity.

#### D. Mean-Squared Error (MSE) Performance of the Doppler Estimators

Since the ultimate purpose of the Doppler estimators is to achieve a good detection performance, in the previous section, we compared the BER performance of a receiver using these estimators. However, when dealing with an estimation problem, it is often desirable to obtain the MSE performance of estimators to compare their accuracy. The MSE results can also be used to explain the receiver BER performance. However, in our scenarios defined by the acoustic environment and trajectory of the transmitter/receiver, it is not directly possible to compute the MSE. The time-varying impulse response  $h(t, \tau)$  is incorporated into the received signal obtained via virtual signal transmission in the Waymark simulator. Therefore, the Doppler parameters associated with the dominant time-varying channel delay  $\tau_d(t)$  are not explicitly available for comparison with their estimates. Moreover, all these parameters are time varying, i.e., there is no single Doppler compression factor or the acceleration parameter for comparison.

To overcome this difficulty, we consider scenarios that are somewhat similar to scenarios described above and, at the same time, make the true Doppler parameters available for comparison with their estimates. In these “synthetic” scenarios, the dominant delay  $\tau_d(t)$  is described by the model (9) with parameters  $a_1$  and  $a_2$  randomly generated. More specifically, the velocity  $v$  and acceleration  $a$  are uniformly distributed in intervals defined by each scenario, and parameters  $a_1$  and  $a_2$  are computed as  $a_1 = -v/c$  and  $a_2 = a/(2c)$ . The impulse response  $\bar{h}(t, \tau)$  is time invariant; it is generated as an FIR impulse response with nonzero taps having relative delays and amplitudes close to those shown in Fig. 7. We run  $N_{MC} = 1000$  simulation trials, with a single measurement of the Doppler compression factor  $a_1$  in each trial, and for every estimator compute the root MSE (RMSE) as

$$\text{RMSE} = \left[ \frac{1}{N_{MC}} \sum_{i=1}^{N_{MC}} \left( a_1^{(i)} - \hat{a}_1^{(i)} \right)^2 \right]^{1/2} \quad (25)$$

where  $a_1^{(i)}$  is the true value of the parameter  $a_1$  in the  $i$ th trial and  $\hat{a}_1^{(i)}$  is its estimate.

The simulation results are shown in Fig. 9. In the scenario with the transmitter moving toward the receiver and summer SSP [see Fig. 9(a)], the velocity  $v$  is randomly generated within the interval  $[4.7, 7.3]$  m/s and the acceleration  $a$  is randomly generated within the interval  $[-0.79, 0.79]$  m/s<sup>2</sup>; the channel is single path. It can be seen that, in the SNR range  $[7, 17]$  dB (used for the analysis of the BER performance) the CAF and MBA estimators significantly outperform the SBA estimator. This is consistent with the BER performance in Fig. 8(a). With the winter SSP [see Fig. 9(b)], the velocity and acceleration are the same as with the summer SSP, but the channel has 7 multipath components in a delay interval of 55 ms, all with equal powers. Again, the MBA and CAF estimator significantly outperform the SBA estimator, which is consistent with the BER performance in Fig. 8(b). With the transmitter moving past the receiver [see Fig. 9(c)], the velocity  $v$  and acceleration  $a$  are randomly generated within intervals  $[-6, 2.2]$  m/s and  $[-0.7, 0.7]$  m/s<sup>2</sup>, respectively. In the channel, there are 5 multipath components within a delay interval of 55 ms with relative powers  $[0.5, 1, 1, 0.5, 0.5]$ . The MSE performance of the CAF and MBA estimators are significantly better than that of the SBA estimator, which matches to the BER performance in Fig. 8(c). Finally, Fig. 9(d) shows the MSE performance in the scenario with the flower circle movement of the transmitter. The velocity  $v$  and acceleration  $a$  are randomly generated within intervals  $[-6.7, -5.3]$  m/s and  $[-0.29, 0.29]$  m/s<sup>2</sup>, respectively. In the channel, there are 9 multipath components within a delay interval of 80 ms with relative powers 0.5 with respect to the multipath component with the longest delay. Now, in the SNR interval  $[7, 17]$  dB, although the CAF and MBA estimators outperform the SBA estimator, the performance gain is not as high as in the previous cases. Note that in this scenario, the acceleration is reduced compared to the previous scenarios, which explain the improved performance of the SBA estimator. This is consistent with the BER performance in Fig. 8(d), where the SBA estimator shows an improvement in the BER performance, though still being inferior to the CAF and MBA estimators.

Fig. 10 shows RMSE of estimation of the parameter  $a_2$  by the MBA method in scenario 1 with the winter SSP. The RMSE is defined as

$$\text{RMSE} = \left[ \frac{1}{N_{MC}} \sum_{i=1}^{N_{MC}} \left( a_2^{(i)} - \hat{a}_2^{(i)} \right)^2 \right]^{1/2} \quad (26)$$

where  $a_2^{(i)}$  is the true value of the parameter  $a_2$  in the  $i$ th trial and  $\hat{a}_2^{(i)}$  is its estimate. In this scenario, the acceleration  $a$  is within the interval  $[-0.79, 0.79]$  m/s<sup>2</sup>, i.e.,  $a_2$  is within an interval  $[-2.6, 2.6] \times 10^{-4}$ . It is seen that at  $\text{SNR} > 3$  dB, the accuracy of the estimates is about 10% of the estimation interval. The RMSE performance in the other scenarios is close to that shown in Fig. 10.

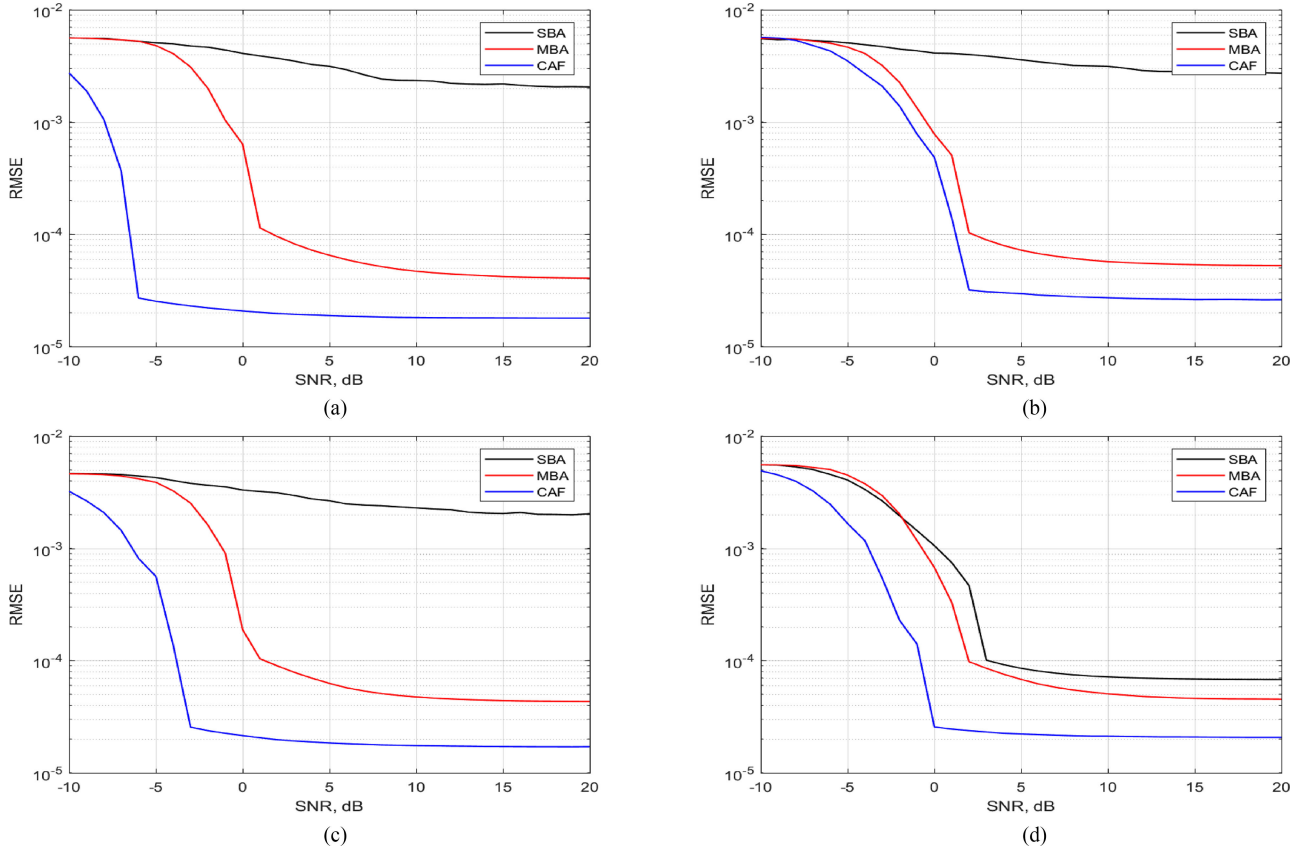


Fig. 9. RMSE performance of estimating the parameter  $a_1$  by the three Doppler estimation methods in four “synthetic” scenarios, corresponding to the scenarios in Figs. 7 and 8 (environment, scenario, distance, data rate). (a) Summer SSP, transmitter moves toward receiver, 10 km, 1/2 b/s/Hz. (b) Winter SSP, transmitter moves toward receiver, 20 km, 1/2 b/s/Hz. (c) Summer SSP, transmitter moves past receiver, 2 km, 1/3 b/s/Hz. (d) Summer SSP, flower circle movement, 5 km, 1/3 b/s/Hz.

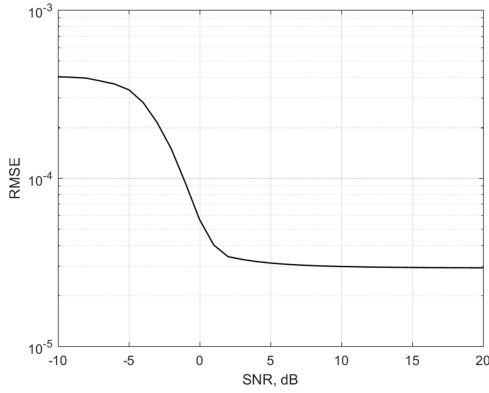


Fig. 10. RMSE performance of estimating the parameter  $a_2$  by the MBA method using (14).

## VI. SEA TRIAL

In this section, we compare the performance of the three Doppler estimation methods using data recorded in a deep-water sea trial, described in [23, session F1–10]. The deep-water SSP is shown in Fig. 11. In the sea trial, 376 guard-free OFDM symbols were transmitted at distances from 81 to 79 km. The transducer was towed at a depth of 200 m by a surface vessel

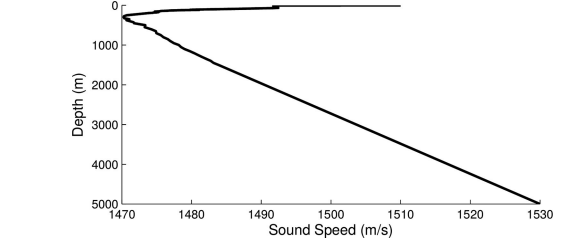


Fig. 11. SSP in the sea trial.

moving at a speed of about 6–7 m/s toward a receiver. Due to the surface waves affecting the towing vessel, the transducer exhibited random oscillations around the main trajectory with an average period about 10 s [23]; this resulted in a (time varying) acceleration between the transmitter and receiver (see Fig. 12). The received omnidirectional hydrophone was slowly drifting at a depth of 400 m. The average SNR during the session is about 11 dB. Fig. 13 shows fluctuations of the channel impulse response in the sea trial, after removing the dominant time-varying delay corresponding to the transmitter speed 6 m/s. It is seen that the channel is characterized by a large number of fast-varying multipath components.

The BER performance is shown in Table I for different coding schemes, characterized by the code polynomial: [3 7], [23 35], or

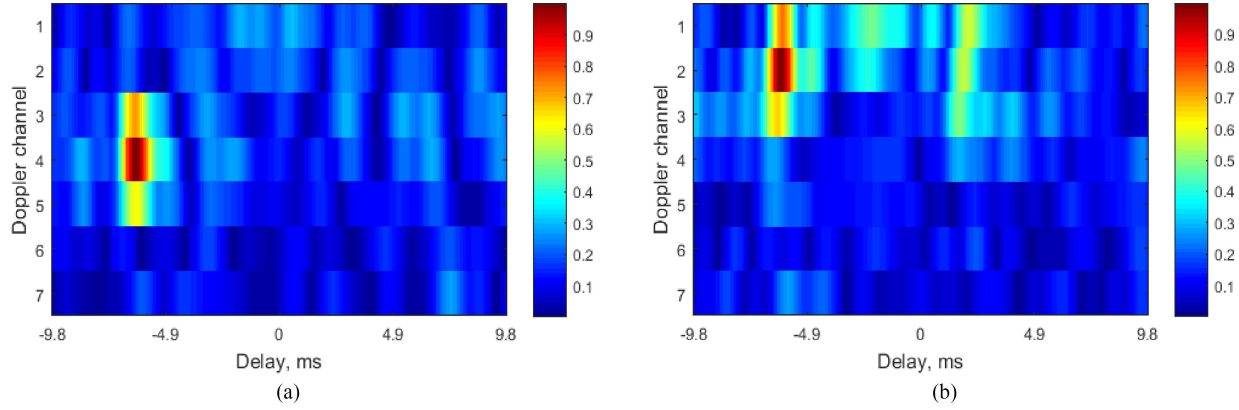


Fig. 12. Examples of the time–frequency autocorrelation function  $|A_{\text{MBA}}(\tau, \Omega_m)|$  in the sea trial. The delay values are shown with respect to the delay  $T_s = 1$  s. (a) Case of low acceleration. (b) Case of high acceleration.

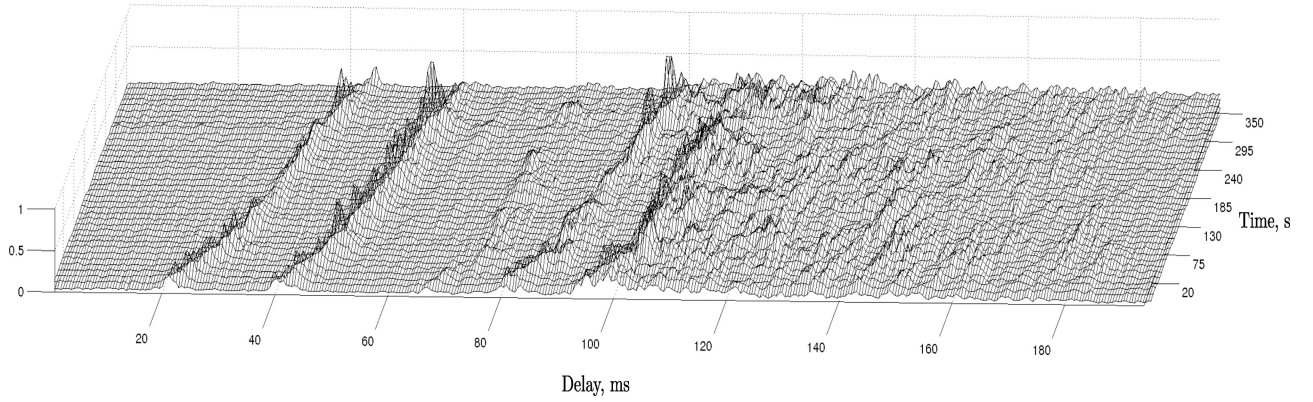


Fig. 13. Fluctuations of the channel impulse response in the sea trial.

TABLE I  
BER PERFORMANCE OF THE RECEIVER WITH THE THREE DOPPLER ESTIMATORS; DATA RATE: 1/2 b/s/Hz

Doppler estimator	Code [3 7]	Code [23 35]	Code [561 753]
CAF	$4.5 \cdot 10^{-3}$	$8.5 \cdot 10^{-4}$	$2.0 \cdot 10^{-5}$
SBA	0.30	0.34	0.37
MBA	$4.8 \cdot 10^{-3}$	$9.2 \cdot 10^{-4}$	0

[561 753] in octal. It can be seen that for all the codes, the MBA method shows a performance similar to that of the CAF method, and it is significantly better than the performance provided by the SBA method. This result is similar to that obtained in Waymark numerical experiments in Section V.

To investigate the detection performance against SNR, we added extra noise recorded in the sea trial to the received signal. Fig. 14 shows the dependence of the BER on SNR for the code [561 753]. It can be seen that the MBA Doppler estimator provides the BER performance similar to that of the CAF method for the whole SNR range. At SNR = 11 dB, the MBA method provides the detection without errors.

The low performance of the SBA method can be explained using Fig. 12(a) and (b) showing  $|A_{\text{MBA}}(\tau, \Omega_m)|$  with seven Doppler sections,  $m = 1, \dots, 7$ . The variable  $m = 4$  cor-

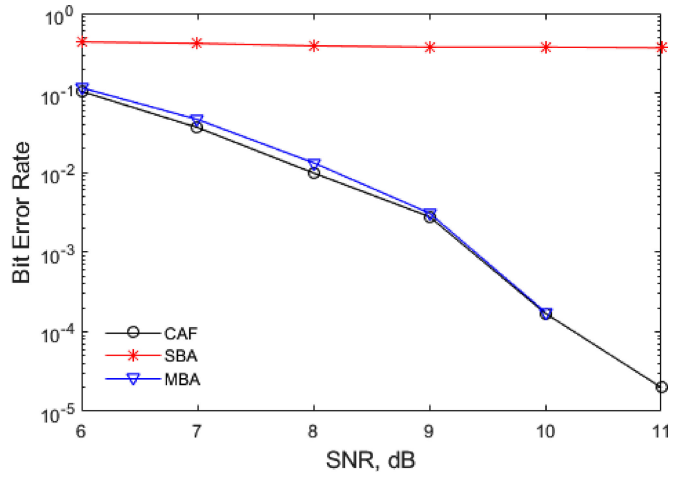


Fig. 14. BER performance of the receiver with the three Doppler estimators in the sea experiment; data rate 1/2 b/s/Hz.

responds to  $\Omega_m = 0$ , i.e.,  $A_{\text{MBA}}(\tau, \Omega_4) = A_{\text{SBA}}(\tau)$ . Fig. 12(a) illustrates a case, when the peak of  $|A_{\text{MBA}}(\tau, \Omega_m)|$  is in the Doppler section  $m = 4$ ; in this case, the SBA method performs as the MBA method. However, in another case, illustrated by Fig. 12(b), the peak is at  $m = 2$ , the SBA method cannot detect

the peak, and, consequently, the detection performance of the receiver is poor.

In this sea trial, the CAF method requires 61 Doppler sections, whereas the MBA method requires only 7 Doppler sections; thus, the complexity of the MBA method is significantly lower. However, the BER performance of the two methods is similar, whereas the SBA method cannot provide reliable detection.

## VII. CONCLUSION

In this paper, we proposed and investigated a new MBA method for Doppler estimation in fast-varying UWA channels. The proposed method not only measures the time compression over the estimation interval, but also the gradient of the time compression, thus allowing more accurate (with time-varying sampling rate) resampling of the received signal to compensate for the Doppler distortions. The proposed method has been compared with a SBA method and a method based on computing the CAF between the received and pilot signals. The results in shallow water simulation scenarios and in the deep-sea trial demonstrate that the proposed method outperforms the SBA method, and it is comparable in the performance to the method based on computation of the CAF. However, the proposed method requires significantly less computations.

## APPENDIX

### A. Derivation of the Multibranch Autocorrelation Method

We now show how the position of the maximum of  $|\rho(\tau, \Omega, \mu)|$

$$\{\tau_{\max}, \Omega_{\max}, \mu_{\max}\} = \arg \max_{\tau, \Omega, \mu} |\rho(\tau, \Omega, \mu)|$$

where  $\rho(\tau, \Omega, \mu)$  is given by (10), relates to the Doppler parameters  $a_1$  and  $a_2$  in (9). Denote the product in the integral (10) as

$$z(t) = \tilde{s}^*(t)\tilde{s}(\mu t + \tau)e^{j\Omega t}. \quad (27)$$

Using (6), we obtain that

$$\begin{aligned} z(t) &= \tilde{s}_0^*[t - \tau_d(t)]\tilde{s}_0[(\mu t + \tau) - \tau_d(\mu t + \tau)] \\ &\times e^{j\omega_c[\tau_d(t) - \tau_d(\mu t + \tau)] + j\Omega t}. \end{aligned} \quad (28)$$

To achieve a maximum of  $|\rho(\tau, \Omega, \mu)|$ , according to the Cauchy–Bunyakovsky–Schwarz inequality [46], the following should be satisfied:

$$\begin{aligned} \tilde{s}_0[t - \tau_d(t)]e^{-j\omega_c[\tau_d(t) - \tau_d(\mu t + \tau)] - j\Omega t} \\ = \beta\tilde{s}_0[(\mu t + \tau) - \tau_d(\mu t + \tau)] \end{aligned} \quad (29)$$

where  $\beta$  is an arbitrary constant independent of time. To satisfy this equality, we need, in particular, to guarantee that the exponent in (29) is independent of time  $t$ . With the approximation of the channel delay  $\tau_d(t)$  as in (9), the component  $\tau_d(t) - \tau_d(\mu t + \tau)$  in the exponent can be represented as

$$\tau_d(t) - \tau_d(\mu t + \tau) = -(a_1\tau + a_2\tau^2) \quad (30)$$

$$+ (a_1 - a_1\mu - 2a_2\mu\tau)t \quad (31)$$

$$+ a_2(1 - \mu^2)t^2. \quad (32)$$

The first (time-independent) term (30) is absorbed in the constant  $\beta$ , and therefore it can be ignored. Below, we will show that the third term (32) can also be ignored. To remove the linear dependence of the exponent on time due to the term (31), the following should be satisfied:

$$\omega_c(a_1 - a_1\mu - 2a_2\mu\tau) + \Omega = 0. \quad (33)$$

From this relationship, we arrive at the following estimate of the parameter  $a_2$ :

$$\hat{a}_2 = \frac{\Omega_{\max} + a_1(1 - \mu_{\max})\omega_c}{2\mu_{\max}\tau_{\max}\omega_c} \quad (34)$$

where instead of  $a_1$  its estimate can be substituted. Note that in many scenarios,  $\mu_{\max} \approx 1$  and, therefore, the estimate in (34) can be simplified and made independent of  $a_1$

$$\hat{a}_2 = \frac{\Omega_{\max}}{2\tau_{\max}\omega_c}. \quad (35)$$

To guarantee (29), we also need to equate arguments of  $\tilde{s}_0(\cdot)$  in both sides of this equation. Thus, we arrive at the relationship

$$t - \tau_d(t) = (\mu t + \tau) - \tau_d(\mu t + \tau) - T_s$$

where we also take into account that the signal  $\tilde{s}_0(t)$  is periodic with the period  $T_s$ . Using (9), this condition takes the form

$$(-a_1\tau - a_2\tau^2 + \tau - T_s) \quad (36)$$

$$+ (a_1 - a_1\mu - 2a_2\mu\tau + \mu - 1) \quad (37)$$

$$+ a_2(1 - \mu^2)t^2 = 0. \quad (38)$$

Due to the time dependence present in this equation, we have to make all the three terms equal zero. Note that the last term (38) can be shown to be close to zero for all  $t \in [-\Theta/2, \Theta/2]$  (see below), and therefore it can be ignored.

Making the first term (36) equal zero results in the following relationship:

$$\begin{aligned} \tau_{\max} &= \frac{1}{2a_2} \left( k - \sqrt{k^2 - 4a_2 T_s} \right) \\ &\approx \frac{T_s}{k} \left( 1 + \frac{a_2 T_s}{k^2} \right) \end{aligned} \quad (39)$$

where  $k = 1 - a_1$ . This approximation is based on the facts that  $k \approx 1$ ,  $a_2 T_s \ll 1$  (see below), and the approximation  $\sqrt{1 - \varepsilon} \approx 1 - \varepsilon/2 - \varepsilon^2/8$ , applicable if  $|\varepsilon| \ll 1$ . If  $a_2 = 0$ , we arrive at the estimate of the parameter  $a_1$  given by

$$\hat{a}_1 = 1 - \frac{T_s}{\tau_{\max}} \quad (40)$$

which is exploited in the SBA estimator. For  $a_2 \neq 0$ , from (39), after some algebra, we arrive at the following estimate of  $a_1$ :

$$\hat{a}_1 = 1 - \frac{T_s}{\tau_{\max}} - \alpha \frac{\Omega_{\max}}{2\omega_c} \quad (41)$$

where  $\alpha = [T_s/(k\tau_{\max})]^2 \approx 1$ .

Making the second term (37) equal zero results in the following relationship:

$$\mu_{\max} = \frac{1}{1 - \frac{2a_2 \tau_{\max}}{k}} \quad (42)$$

where instead of  $a_2$  its estimate  $\hat{a}_2$  can be used. By substituting  $\hat{a}_2$  from (34) into (42), we obtain

$$\mu_{\max} = 1 + \frac{\Omega_{\max}}{\omega_c}. \quad (43)$$

Thus,  $\mu_{\max}$  can be found from  $\Omega_{\max}$ . This simplifies the Doppler estimation. According to (11), the statistic  $|\rho(\tau, \Omega, \mu)|$  needs to be computed at a 3-D grid. However, as  $\mu_{\max}$  and  $\Omega_{\max}$  are interdependent, only a 2-D grid over  $(\tau, \Omega)$  is sufficient.

Previously, the term  $a_2(1 - \mu^2)t^2$  has been ignored for  $t \in [-\Theta/2, \Theta/2]$  in (32) and (38); we now justify this step in our derivation. In many applications, it can be assumed that  $a < 1 \text{ m/s}^2$  [22], [29], [35]. Assuming also that  $\Delta$  is the time-correlation interval of the signal  $\tilde{s}_0(t)$ , which is given by  $\Delta \approx 1/F$ , the term  $a_2t^2(1 - \mu^2)$  can be ignored if

$$\xi = |a_2t^2(1 - \mu_{\max}^2)| \ll \Delta \approx \frac{1}{F}.$$

From (42), taking into account that for  $|\varepsilon| \ll 1$ ,  $(1 - \varepsilon)^{-2} \approx 1 + 2\varepsilon$  and  $\tau_{\max} \simeq T_s/k$ , we approximately have

$$1 - \mu_{\max}^2 \cong -\frac{4a_2T_s}{k^2}.$$

Therefore, it is sufficient to require that

$$\xi_{\max} = \max_{t \in [-\Theta/2, \Theta/2]} \xi = \frac{a^2\Theta^2T_sF}{4c^2} \ll 1.$$

In our experimental scenarios, we have  $\Theta = 1 \text{ s}$ ,  $T_s = 1 \text{ s}$ ,  $F = 1024 \text{ Hz}$ ,  $c = 1500 \text{ m/s}$ , and  $a < 1 \text{ m/s}^2$ . For all these scenarios,  $\xi_{\max} < 10^{-4} \ll 1$ ; thus, this requirement is satisfied with a significant margin.

When deriving (41), it was assumed that  $a_2T_s \ll 1$ . Indeed, in our scenarios with  $a < 1 \text{ m/s}^2$ ,  $a_2T_s = aT_s/(2c) < 1/3000 \ll 1$ , i.e., the assumption is satisfied with a significant margin.

We now analyze a possibility of setting  $\mu = 1$  in (11) to further simplify the Doppler estimator. Such setting is possible if

$$|\Theta - \Theta\mu_{\max}| < \Delta \approx \frac{1}{F}$$

or  $\Theta|1 - \mu_{\max}| < 1$ , i.e., if the signal compression due to the factor  $\mu_{\max}$  over the observation interval  $\Theta$  does not exceed the signal autocorrelation interval  $\Delta$ . For our scenarios, from (42) we obtain

$$\Theta|1 - \mu_{\max}| < 0.67 < 1$$

i.e., this requirement is satisfied and we can set  $\mu = 1$ . Indeed, with higher values of the measurement interval  $\Theta$  and the frequency bandwidth  $F$ , one of the components in (10) needs to be prescaled with a compression factor  $\mu$  related to the frequency  $\Omega$  as  $\mu = 1 + \Omega/\omega_c$ .

## B. Complexity Analysis

Below, we analyze the complexity of the CAF, MBA, and SBA methods in terms of real-valued multiply-accumulate (MAC) operations, which is the typical operation in DSP processors [47], [48].

**1) Cross-Ambiguity Function Method:** The computation of one Doppler section of the CAF requires the resampling, frequency correction, FFT, multiplication by the pilot sequence, IFFT, computation of (square) magnitudes, and finding a maximum (see Fig. 3). For the resampling, the linear interpolation is used, which requires four MACs for one complex-valued baseband sample. The frequency correction requires one complex-valued multiplication (4 MACs) per sample. The linear interpolation and frequency correction need to be done  $N_s N_\tau$  times. The FFT and IFFT of size  $N_s N_\tau$  are required. Assuming that the FFT/IFFT is implemented using the split-radix algorithm [49], its complexity is  $P_{\text{FFT}} = 3N_s N_\tau \log_2(N_s N_\tau)$  MACs. For multiplication by the (real-valued) pilot sequence,  $2N_s$  MACs are required. Instead of computing the CAF magnitude, it is more practical to compute its square magnitude, which requires  $2N_s N_\tau$  MACs. Finding the magnitude maximum requires  $N_s N_\tau$  MACs per Doppler section. In total, the computation of one Doppler section in the CAF Doppler estimator requires

$$P_{\text{CAF}} = 11N_s N_\tau + 2N_s + 6N_s N_\tau \log_2(N_s N_\tau) \sim \text{MACs}.$$

With  $N_\tau = 2$  and  $N_s = 1024$ , the complexity is  $P_{\text{CAF}} \approx 160 \cdot 10^3$  MACs. It can be seen that the complexity is dominated by computing the FFT and IFFT.

**2) Multibranch Autocorrelation and Single-Branch Autocorrelation Methods:** The computation of one Doppler section in the MBA method requires the frequency shift and computation of the autocorrelation according to (19), computation of (square) magnitudes, and finding the maximum. The frequency shift requires  $4N_s N_\tau$  MACs. The further complexity will depend on the search area over the delay  $\Lambda = [T_s - \tau_M, T_s + \tau_M]$ . If the search area  $\Lambda$  is large, the autocorrelation is preferably computed using FFT and IFFT; on average (if FFTs in the consecutive estimation intervals are reused), for such computation, one FFT and one IFFT are required. The autocorrelation computation requires  $4N_s N_\tau + 2P_{\text{FFT}}$  MACs, where  $4N_s N_\tau$  MACs are needed for multiplication of the FFT outputs. In total, when using FFTs for computation of the autocorrelation, the complexity of computing one Doppler section in the MBA method is given by

$$P_{\text{MBA}} = 8N_s N_\tau + 2P_{\text{FFT}} + 3|\Lambda| \sim \text{MACs},$$

where  $|\Lambda|$  denotes the size (cardinality) of  $\Lambda$  and the last term is the complexity of computing the square magnitudes and finding the maximum; note that typically  $|\Lambda| \ll N_s N_\tau$ . In our scenarios, with a maximum speed of  $\pm 7.3 \text{ m/s}$ , we have  $\tau_M \approx 4.9 \text{ ms}$ ; thus,  $|\Lambda| = 2\tau_M N_s N_\tau / T_s \approx 40$ . With  $N_\tau = 2$  and  $N_s = 1024$ , the complexity is  $P_{\text{MBA}} \approx 152 \cdot 10^3$  MACs. It can be seen that similarly to the CAF computation, the MBA computation is dominated by the complexity of computing the FFT and IFFT, and therefore  $P_{\text{MBA}} \approx P_{\text{CAF}}$ .

However, if the search area  $\Lambda$  is small, the direct computation according to (19) could be less complicated. The direct computation of the autocorrelation requires  $4|\Lambda|N_s N_\tau$  MACs. In this case, the total complexity is

$$P_{\text{MBA}} = 4N_s N_\tau + 4|\Lambda|N_s N_\tau + 3|\Lambda| \text{ MACs.}$$

With  $N_\tau = 2$ ,  $N_s = 1024$ , and  $|\Lambda| = 40$ , the complexity is  $P_{\text{MBA}} \approx 336 \cdot 10^3$  MACs, which is still higher than the complexity of the computation using FFTs. Thus, in our scenarios, the preferable implementation of the MBA method is the one based on FFTs, and therefore, the complexity of computation of one Doppler section  $P_{\text{MBA}}$  is almost the same as  $P_{\text{CAF}}$ .

The SBA method is a particular case of the MBA method, and its complexity  $P_{\text{SBA}}$  is similarly dominated by the computation of the FFT and IFFT. Therefore, we have  $P_{\text{SBA}} \approx P_{\text{MBA}} \approx P_{\text{CAF}}$ , and to compare the complexity of the Doppler estimators, it is enough to compare the number of Doppler sections  $2N_d + 1$  required by the estimators. In the SBA method,  $N_d = 0$ , and only one Doppler section is used. For scenarios, considered in this paper, the value of  $N_d$  in the MBA method is significantly smaller than  $N_d$  in the CAF method. Thus, the complexity of the MBA method is significantly lower than the CAF complexity.

## REFERENCES

- [1] Y. V. Zakharov and J. Li, "Autocorrelation method for estimation of Doppler parameters in fast-varying underwater acoustic channels," in *Proc. Underwater Acoust., Conf. Exhib.*, Crete, Greece, 2015, pp. 1–4.
- [2] B. S. Sharif, J. Neasham, O. R. Hinton, and A. E. Adams, "A computationally efficient Doppler compensation system for underwater acoustic communications," *IEEE J. Ocean. Eng.*, vol. 25, no. 1, pp. 52–61, Jan. 2000.
- [3] B. Li, S. Zhou, M. Stojanovic, L. Freitag, and P. Willett, "Multicarrier communication over underwater acoustic channels with nonuniform Doppler shifts," *IEEE J. Ocean. Eng.*, vol. 33, no. 2, pp. 198–209, Apr. 2008.
- [4] C. R. Berger, S. Zhou, J. C. Preisig, and P. Willett, "Sparse channel estimation for multicarrier underwater acoustic communication: From subspace methods to compressed sensing," *IEEE Trans. Signal Process.*, vol. 58, no. 3, pp. 1708–1721, Mar. 2010.
- [5] S. Yerramalli and U. Mitra, "Optimal resampling of OFDM signals for multiscale–multilag underwater acoustic channels," *IEEE J. Ocean. Eng.*, vol. 36, no. 1, pp. 126–138, Jan. 2011.
- [6] G. Eynard and C. Laot, "Blind Doppler compensation scheme for single carrier digital underwater communications," in *Proc. IEEE OCEANS Conf.*, 2008, pp. 1–5.
- [7] M. Johnson, L. Freitag, and M. Stojanovic, "Improved Doppler tracking and correction for underwater acoustic communications," in *Proc. IEEE Int. Conf. Acoust., Speech, Signal Process.*, 1997, vol. 1, pp. 575–578.
- [8] B. Li, S. Zhou, M. Stojanovic, L. Freitag, and P. Willett, "Non-uniform Doppler compensation for zero-padded OFDM over fast-varying underwater acoustic channels," in *Proc. IEEE OCEANS Eur. Conf.*, 2007, pp. 1–6.
- [9] M. Stojanovic and J. Preisig, "Underwater acoustic communication channels: Propagation models and statistical characterization," *IEEE Commun. Mag.*, vol. 47, no. 1, pp. 84–89, Jan. 2009.
- [10] C. Liu, Y. V. Zakharov, and T. Chen, "Doubly selective underwater acoustic channel model for a moving transmitter/receiver," *IEEE Trans. Veh. Technol.*, vol. 61, no. 3, pp. 938–950, Mar. 2012.
- [11] J. S. Dhanoa and R. F. Ormondroyd, "Combined differential Doppler and time delay compensation for an underwater acoustic communication system," in *Proc. MTS/IEEE OCEANS Conf.*, 2002, vol. 1, pp. 581–587.
- [12] S. F. Mason, C. R. Berger, S. Zhou, and P. Willett, "Detection, synchronization, and Doppler scale estimation with multicarrier waveforms in underwater acoustic communication," *IEEE J. Sel. Areas Commun.*, vol. 26, no. 9, pp. 1638–1649, Dec. 2008.
- [13] A. Y. Kibangou, C. Siclet, and L. Ros, "Joint channel and Doppler estimation for multicarrier underwater communications," in *Proc. Int. Conf. Acoust., Speech, Signal Process.*, 2010, pp. 5630–5633.
- [14] X. Xu, Z. Wang, S. Zhou, and L. Wan, "Parameterizing both path amplitude and delay variations of underwater acoustic channels for block decoding of orthogonal frequency division multiplexing," *J. Acoust. Soc. Amer.*, vol. 131, no. 6, pp. 4672–4679, 2012.
- [15] Z. Wang, S. Zhou, J. C. Preisig, K. R. Pattipati, and P. Willett, "Clustered adaptation for estimation of time-varying underwater acoustic channels," *IEEE Trans. Signal Process.*, vol. 60, no. 6, pp. 3079–3091, Jun. 2012.
- [16] N. Santos, A. Matos, and N. Cruz, "Navigation of an autonomous underwater vehicle in a mobile network," in *Proc. IEEE OCEANS Conf.*, 2008, Sep. 15–18, 2008, pp. 1–5.
- [17] R. N. Smith, Y. Chao, B. H. Jones, D. A. Caron, P. P. Li, and G. S. Sukhatme, "Trajectory design for autonomous underwater vehicles based on ocean model predictions for feature tracking," in *Field and Service Robotics*. New York, NY, USA: Springer-Verlag, 2010, pp. 263–273.
- [18] B. He, H. Zhang, C. Li, S. Zhang, Y. Liang, and T. Yan, "Autonomous navigation for autonomous underwater vehicles based on information filters and active sensing," *Sensors*, vol. 11, no. 11, pp. 10 958–10 980, 2011.
- [19] F. García-Córdoba and A. Guerrero-González, "Intelligent navigation for a solar powered unmanned underwater vehicle," *Int. J. Advanced Robot. Syst.*, vol. 10, no. 4, pp. 185–198, 2013.
- [20] O. Gal, "Unified trajectory planning algorithms for autonomous underwater vehicle navigation," *ISRN Robot.*, vol. 2013, 2013, Art. no. 329591.
- [21] J. McColgan and E. W. McGookin, "Coordination of multiple biomimetic autonomous underwater vehicles using strategies based on the schooling behaviour of fish," *Robotics*, vol. 5, no. 1, pp. 2–25, 2016.
- [22] N. Parrish, S. Roy, and P. Arabshahi, "Symbol by symbol Doppler rate estimation for highly mobile underwater OFDM," in *Proc. 4th ACM Int. Workshop Underwater Netw.*, Berkeley, CA, USA, Nov. 2009, pp. 1–8.
- [23] Y. V. Zakharov and A. K. Morozov, "OFDM transmission without guard interval in fast-varying underwater acoustic channels," *IEEE J. Ocean. Eng.*, vol. 40, no. 1, pp. 144–158, Jan. 2015.
- [24] T. Yang, "Underwater telemetry method using Doppler compensation," U.S. Patent 6 512 720, Jan. 28, 2003.
- [25] L. Wan, Z. Wang, S. Zhou, T. C. Yang, and Z. Shi, "Performance comparison of Doppler scale estimation methods for underwater acoustic OFDM," *J. Elect. Comput. Eng.*, vol. 2012, pp. 1–11, 2012.
- [26] M. Stojanovic, J. A. Catipovic, and J. G. Proakis, "Phase-coherent digital communications for underwater acoustic channels," *IEEE J. Ocean. Eng.*, vol. 19, no. 1, pp. 100–111, Jan. 1994.
- [27] T. J. Riedl and A. C. Singer, "Broadband Doppler compensation: Principles and new results," in *Proc. Conf. Rec. 45th Asilomar Conf. Signals, Syst. Comput.*, 2011, pp. 944–946.
- [28] K. A. Perrine, K. F. Nieman, T. L. Henderson, K. H. Lent, T. J. Brudner, and B. L. Evans, "Doppler estimation and correction for shallow underwater acoustic communications," in *Proc. IEEE Conf. Rec. 44th Asilomar Conf. Signals, Syst. Comput.*, 2010, pp. 746–750.
- [29] T. Arikan, T. Riedl, A. Singer, and J. Younce, "Comparison of OFDM and single-carrier schemes for Doppler tolerant acoustic communications," in *Proc. IEEE OCEANS Conf.*, Genova, Italy, 2015, pp. 1–7.
- [30] Y. V. Zakharov and V. P. Kodanov, "Experimental study of an underwater acoustic communication system with pseudonoise signals," *J. Acoust. Phys.*, vol. 40, no. 9, pp. 707–715, 1994.
- [31] Y. V. Zakharov and V. P. Kodanov, "Doppler scattering adaptive reception in a hydroacoustic communication channel," *J. Acoust. Phys.*, vol. 41, no. 2, pp. 219–223, 1995.
- [32] G. Jourdain, "Characterization of the underwater channel application to communication," in *Issues in Acoustic Signal-Image Processing and Recognition*. New York, NY, USA: Springer-Verlag, 1983, pp. 197–209.
- [33] S. M. Kay and S. B. Doyle, "Rapid estimation of the range-Doppler scattering function," *IEEE Trans. Signal Process.*, vol. 51, no. 1, pp. 255–268, Jan. 2003.
- [34] A. E. Abdelkareem, B. S. Sharif, C. C. Tsimenidis, J. A. Neasham, and O. R. Hinton, "Low-complexity Doppler compensation for OFDM-based underwater acoustic communication systems," in *Proc. IEEE OCEANS Conf.*, Spain, 2011, pp. 1–6.
- [35] A. E. Abdelkareem, B. S. Sharif, and C. C. Tsimenidis, "Adaptive time varying Doppler shift compensation algorithm for OFDM-based underwater acoustic communication systems," *Ad Hoc Netw.*, vol. 45, pp. 104–119, 2016.
- [36] J. C. Peterson and M. B. Porter, "Ray/beam tracing for modeling the effects of ocean and platform dynamics," *IEEE J. Ocean. Eng.*, vol. 38, no. 4, pp. 655–665, Oct. 2013.
- [37] P. Qarabiqi and M. Stojanovic, "Statistical characterization and computationally efficient modeling of a class of underwater acoustic communication channels," *IEEE J. Ocean. Eng.*, vol. 38, no. 4, pp. 701–717, Oct. 2013.

- [38] M. B. Porter, "The BELLHOP manual and users guide: Preliminary draft," Heat, Light, Sound Res., Inc., La Jolla, CA, USA, Tech. Rep. Rays/HLS-2010-1, 2011.
- [39] B. Henson, J. Li, Y. V. Zakharov, and C. Liu, "Waymark baseband underwater acoustic propagation model," in *Proc. Underwater Commun. Netw.*, 2014, pp. 1–5.
- [40] B. Henson, "Waymark based underwater acoustic channel model," Apr. 29 2017. [Online]. Available: <https://www.york.ac.uk/electronic-engineering/research/communication-technologies/underwater-networks/resources/>
- [41] Y. V. Zakharov and A. K. Morozov, "Adaptive sparse channel estimation for guard-free OFDM transmission in underwater acoustic channels," in *Proc. UAC*, Jun. 2013, pp. 1–4.
- [42] J. G. Proakis, *Digital Communications*. New York, NY, USA: McGraw-Hill, 1995.
- [43] W. W. S. Wei, *Time Series Analysis*. Reading, MA, USA: Addison-Wesley, 1994.
- [44] R. M. Hamson and R. M. Heitmeyer, "Environmental and system effects on source localization in shallow water by the matched-field processing of a vertical array," *J. Acoust. Soc. Amer.*, vol. 86, no. 5, pp. 1950–1959, 1989.
- [45] D. F. Gingras, "Robust broadband matched-field processing: Performance in shallow water," *IEEE J. Ocean. Eng.*, vol. 18, no. 3, pp. 253–264, Jul. 1993.
- [46] I. S. Gradshteyn and I. M. Ryzhik, *Table of Integrals, Series, and Products*. San Diego, CA, USA: Academic, 2000.
- [47] L. J. Karam *et al.*, "Trends in multicore DSP platforms," *IEEE Signal Process. Mag.*, vol. 26, no. 6, pp. 38–49, Nov. 2009.
- [48] A. Bateman and S. I. Paterson, *The DSP Handbook*. Englewood Cliffs, NJ, USA: Prentice-Hall, 2002.
- [49] P. Duhamel and H. Hollmann, "Split-radix FFT algorithm," *Electron. Lett.*, vol. 20, no. 1, pp. 14–16, 1984.



**Jianghui Li** (S'16) received the B.S. degree in communications engineering from Huazhong University of Science and Technology, Wuhan, China, in 2011 and the M.Sc. degree in communications engineering and the Ph.D. degree with receiving the K. M. Stott Prize for excellent research in electronics engineering from the University of York, York, U.K., in 2013 and 2017, respectively. From 2011 to 2012, he was a Research Assistant with the Chinese Academy of Sciences, Beijing, China. Since 2017, he has been a Research Fellow with the University of Southampton and National Oceanography Centre, Southampton, U.K. His current research interests include adaptive signal processing, underwater acoustics, and wireless communications.



**Yuriy V. Zakharov** (SM'07) received the M.Sc. and Ph.D. degrees in electrical engineering from the Power Engineering Institute, Moscow, Russia, in 1977 and 1983, respectively.

From 1977 to 1983, he was with the Special Design Agency in the Moscow Power Engineering Institute. From 1983 to 1999, he was with the N. N. Andreev Acoustics Institute, Moscow. From 1994 to 1999, he was with Nortel as a DSP Group Leader. Since 1999, he has been with the Communications Research Group, University of York, York, U.K., where he is currently a Reader in the Department of Electronics. His research interests include signal processing, communications, and acoustics.



**Benjamin Henson** (S'16) received the M.Eng. degree in electronic engineering and the M.Sc. degree in natural computation in 2001 and 2011, respectively, from the University of York, York, U.K., where he is currently working toward the Ph.D. degree in electronic engineering in the Communications Research Group, Department of Electronics.

From 2002 to 2008, he was an Engineer at Snell & Wilcox, Ltd., designing broadcast equipment. From 2008 to 2009, he was with SRD, Ltd., working on image sonar designs. Then, from 2011 to 2013, he worked on laser measurement equipment for Renishaw, plc. His interests include signal and image processing and acoustics.